Molecular BioSystems

Accepted Manuscript

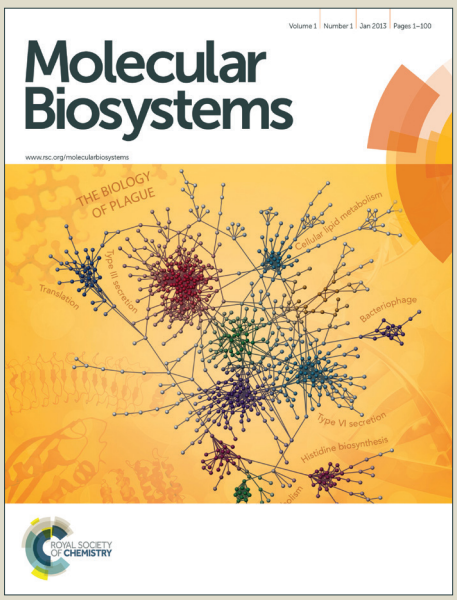

ROYAL SOCIETY OF CHEMISTRY

www.rsc.org/molecularbiosystems

L-asparaginase as a new molecular target against leishmaniasis: insights about mechanism of action and structure-based inhibitor design

Jasdeep Singh[a§], Ankit Srivastava[a§], Pravin Jha[b], Kislay K Sinha[b], Bishwajit Kundu[a]*

Kusuma School of Biological Sciences, Indian Institute of Technology Delhi, New Delhi-110016, India

National Institute of Pharmaceutical Education & Research, EPIP Complex, Hajipur, Vaishali-844102, India

Abstract

L-asparaginases belong to a family of amidohydrolases that catalyze L-asparagine into L-aspartic acid and ammonia. Although bacterial L-asparaginases have been used extensively as anti-leukemic agents, their possible role as potential drug target for pathogenic organisms has not been explored. The presence of genes coding for putative L-asparaginase enzymes in *Leishmania donovani* genome hinted towards specific role of these enzymes in extending survival benefit to the organism. To investigate whether this enzyme can serve as a potential drug target against Leishmania pathogen, we obtained structural models of one of the putative Leishmania L-asparaginase I (LdAI). Using an integrated computational approach involving molecular modelling, docking and molecular dynamics simulations, we found crucial differences between catalytic residues of LdAI as compared to bacterial L-asparaginases. The deviation from canonical acid-base pair at triad I, along with structural reorganization of a β-hairpin loop in the presence of substrate, indicated an altogether new mechanism of action of the LdAI enzyme. Moreover, the finding of compositional and functional differences between LdAI and human asparaginase was used as a criterion to identify specific small molecule inhibitors. Through virtual screening of a library of 11,438 compounds, we report five compounds that showed favorable interactions with the active pocket of LdAI, without adversely effecting human asparaginase. One of these compounds when tested on cultured Lesimania promastigotes displayed promising Leishmanicidal effect. Overall, our work not only provides first hand mechanistic insights of LdAI but also propose five strongly active compounds which may prove as effective anti-leishmaniasis molecules.

---

§These authors have equal contribution

* Corresponding author: Phone: 911126591037, Fax: 911126597523

Email address: bkundu@bioschool.iitd.ac.in

Key words: Leishmania; L-asparaginase; molecular modelling, molecular docking; molecular dynamics; inhibitor.

1. Introduction

Leishmaniasis is a prominent pathogenic disease in tropical countries caused by the protozoan parasites *Leishmania spp.* [1-3]. Although *Leishmania* can affect various tissues, the visceral infection (known as kala-azar) is most lethal, as at later stages of infection the pathogen severely compromises the host immune response [4-6]. During infection, this pathogen usually begins infiltrating the phagocytic cells, forms phagolysosomes, proliferate via complex host-parasite interactions and eventually surpass host immune responses by strategically evading destruction by the host cells [7, 8]. Forward line chemotherapy of leishmaniasis includes administration of pentavalent antimonials, anti-fungal antibiotic and aromatic dimidines [9-13]. Some of the anti-retro viral drugs and immunomodulators have recently been introduced in conjunction with chemotherapy to potentiate anti-leishmanial effects [14-17]. Besides being expensive and highly toxic, acquisition of drug resistance by the protozoa against the chemotherapeutics is a major threat, necessitating the identification of newer drugs [18-20]. In the absence of effective vaccines, inhibitors designed against pathogen-specific protein targets may prove to be most appropriate, next generation, anti-leishmaniasis drugs.

Good volume of literature supports the employment of comparative proteome and genome analysis for finding effective drug targets against protozoan pathogens [21,22]. Recently, an L-asparagine synthase has been found important in rendering survival benefit to *Leishmania,* and hence has been proposed as a potential drug target [23]. Whole proteome BLAST showed that amongst various protozoan pathogens, a distinct genomic region coding for

putative L-asparaginase is present only in *Leishmania*, *Giardia* and *Trichomonas spp*. L-Asparaginases belong to amidohydrolase class of enzymes and have been used as effective anti-leukemic agent [24]. Its specific role in pathogenic protozoans has not been evaluated. An earlier report suggests that the amino acid L-asparagine (substrate for L-asparaginase) poses an inhibitory control over leishmanial auto-phagosomal pathway [25]. In a recent report it has been shown that the L-asparaginase of *Mycobacterium tuberculosis (M tb)* renders survival benefit to the pathogen by reducing the acidic environment inside the host cell [26]. Since a phagolysomal fusion mechanism is common for the establishment of infection by both *M. tuberculosis* and *Leishmania donovani*, we hypothesized that LdAI might be serving identical neutralizing function for the survival of *Leishmania* inside the host. While this requires experimental verification, we present first hand computational analysis of the putative LdAI with a preliminary in *vitro* testing data to support our hypothesis.

Our data shows characteristic deviations of LdAI from the other known L-asparaginases in its catalytic site composition, hinting towards a novel mechanism of action. Based on this we identified five potential inhibitors of LdAI from a large library of compounds. We confirmed our data about active site mechanism and the binding poses of the reported inhibitors using Molecular docking and MD simulations. Our results strongly support the uniqueness of LdAI that can be exploited as a potential and specific protein target against leishmaniasis. We hence, believe that the information reported in our study will be critical and helpful in designing new and efficacious inhibitors against lieshmaniasis in future.

2. Materials and methods

2.1 Material retrieval and sequence alignment

Protein sequences of L-asparaginase I (Uniprot: P0A962) and II (Uniprot: P00805) from *E. coli* (EcAI and EcAII) were retrieved from UniProtKB and a BLASTp analysis of these sequences was done to identify putative L-asparaginase genes associated with enteric pathogens. To identify residues in the catalytic triads of different asparaginases, multiple sequence alignment of

various sequences *Lieshmania spp.* (*Leishmania donovani*, *Leishmania infantum*, *Leishmania major*, *Leishmania mexicana*, *Leishmania braziliensis*) was done along with L-asparaginases from *E. coli* using CLUSTALW2 [27-29].

2.2 Model building and evaluation

The *Leishmania donovani* L-asparaginase (LdAI) structure was built using comparative modelling from its primary sequence (Uniprot: E9BC85). Initially, the LdAI sequence was submitted to I-TASSER [30,31] (Iterative Threading Assembly Refinement) server that generates atomic models based on multiple threading alignments of sequences with continuous Z-score assignments. Following this, all the continuously aligned fragments are assembled using the conformational constraints of the template structures. In the next step, structural matching of predicted models with known protein structures from the RCSB Protein Data Bank (PDB) is performed and C-scores are assigned based on relative clustering structural density and consensus significance. Finally, the best model based on C-scores among the top five modelled structures was chosen for further studies. The inspection of phi/psi angles using Ramachandran plot and energy criterion comparison was done to validate the overall quality of the chosen model using PROCHECK and ProSA [32, 33] programs, respectively.

2.3 Virtual Screening of compounds against LdAI

Virtual screening (VS) was carried out using a composite ligand based and receptor based approach. Firstly, the filtering conditions for virtual screening of approximately 23 million compounds from the ZINC database were applied on the basis of physicochemical properties of the enzyme substrate, L-asparagine. These screened ligands were further filtered using the AutoDock Vina [34] docking engine, adopted for a receptor-based virtual screening via the iDOCK modification [35]. The docking grid was defined to encompass the active site of LdAI (residues 11,16,21,89,91 in modelled structure). Various conformational orientations of ligands were analyzed and ranked based on their binding scores. Only the top 100 compounds with highest binding scores (>L-asp; score -5.3, 100th compound ; score -5.7) were selected based on

the Lipinski's rule of five [36] and respective iDock scores. The absorption, distribution, metabolism, excretion and toxicity (ADMET) properties constitute crucial part of pharmacokinetic profile of drug candidates. The druggability of candidate compounds and their clinical effectiveness is based on their ADMET profile. Thus, only the top 20 drug-like compounds were retained based on predicted low toxicity values using admetSAR [37]. The five reported pharmacokinetic parameters and their evaluation models are described in the supplementary methods.

2.4 Re-docking and free energy calculation

For eliminating the possibility of inhibitory effect of the selected ligands on the human asparaginase isoform (Type-III L-asparaginase, HLA), binding of the top 20 admetSAR filtered compounds was re-assessed using Molecular Operating Environment (MOE) v2009.10 [38]. MOE utilizes a Monte Carlo simulated annealing process from a set of energy grids at the active site pocket of the protein. As compared to other docking algorithms such as AutoDock [39], Glide [40] and Gold [41], MOE can produce ligand poses close to original conformers with minimum RMSD. Besides, it also samples larger conformational spaces which are close to native pose of the ligands upon interaction with receptors [42]. Hence, MOE was employed for precise free energy calculations. The ligands were re-docked using MOE onto the active pockets of LdAI and HLA using the above described active site grid parameters. Finally, triangular matching placement method was employed to generate poses by aligning ligand triplets of atoms with triplets of receptor site points. London dG scoring function was used to retain most favorable poses of ligand conformations.

The free energy of ligand binding from a given pose is defined as:

$$\boldsymbol{\Delta G = c + E_f + \sum_{h-bonds} CbFb + \sum_{m-ligand} CmFm + \sum_{atoms\ i} \Delta Di}$$

where, *c* represents the average gain/loss of rotational and translational entropy, E_f is the energy due to the change in flexibility of the ligand upon binding, Fb measures geometric

imperfections of hydrogen bonds, Cb is the energy of an ideal hydrogen bond, Fm measures geometric imperfections of metal ligations, Cm is the energy of an ideal metal ligation; and *Di* represents desolvation energy of i^{th} atom.

Difference in desolvation energies are calculated as:

$$\boldsymbol{\Delta Di = c_i R_i^3 \{ \iiint_{u \notin A \cup B}^{\cdot} |u|^{-6}\, dU}$$

where, *A* and *B* are the protein and ligand volumes with atom *i* belonging to volume *B*; R_i is the solvation radius of atom *i* and c_i is the desolvation coefficient of atom *i*. The best five conformations were evaluated using the Generalized Born solvation model ranked by higher binding free energy to LdAI in comparison to HLA.

$$\boldsymbol{E_{solvation=-w_{sol}} W\left(d^{-1} - d_x^{-1}\right) \frac{e^2}{4\Pi\varepsilon} \frac{1}{2} \sum_{i-1}^{n} \sum_{j-1}^{n} \cdot \frac{q_i q_j \sqrt{G_i G_j}}{\sqrt{y_{ij} + \exp(-y_{ij})/4}} s(r_{ij}) T_{ij}}$$

where, w_{sol} and *W* are weights, *d* is the dielectric constant in the interior of the solute, d_x is the dielectric constant of the solvent and *s* and *T* are as in the van der Waals energy. G_i is the self energy of atom i, defined as:

$$\boldsymbol{G_i = \frac{-1}{2} \sqrt[3]{\frac{1}{R_i^3}} - V_i, \quad V_i \approx \iiint_{x \in solute}^{\cdot} \sqrt[-6]{|x - x_i|}\, |\delta(|x - x_i| > R_i) dx}$$

where, R_i is the solvent model radius of atom *i* and V_i is an approximation to the Born Integral. Subsequently, the resulting five LdAI-inhibitor complexes were subjected to molecular dynamics simulations to ascertain stability of these complexes. The holo-enzyme complex of LdAI and its substrate L-asparagine was similarly created by docking the substrate into the active site of the enzyme.

2.5 Molecular dynamics simulations

MD simulations were carried using GROMACS package v4.5.5. The GROMOS 53A6 force field [43] was employed for analysing apo-LdAI (without substrate) and holo-LdAI (with substrate or inhibitors). The Ligand topologies were generated using PRODRG [44]. In separate

set of simulations, apo-LdAI, holo-LdAI and the five LdAI-ligand complexes were placed in cubical boxes, equidistantly at 15Å distance from box edges. Following this, hydrogen atoms were added using pdb2gmx module of GROMACS and were constrained using LINCS algorithm. With periodic boundary conditions applied in all three dimensions, protein was explicitly solvated using TIP3P water system and appropriate counter ions were added to neutralize the system. Solvated system was first energy minimized by steepest descent method (2000 steps) followed by conjugant gradient (1000 steps) method. In two steps of 400ps each, the systems were equilibrated in an NVT ensemble followed an NPT ensemble. Particle mesh Ewald (PME) method was employed to treat long-range electrostatic interactions with cut off radius of 10Å.The system temperature of 300K was kept constant by modified Berendsen coupling. The Leap frog integration was used for velocity generation with 2 fs time step. The structural coordinates were recorded at 4 ps intervals in total of 15 ns simulations for apo-LdAI and holo-LdAI along with 10 ns each for LdAI-ligand complexes. The resulting trajectories were later analyzed for RMSD, Solvent accessible surface area, Radius of gyration and Energy. The structural coordinates were analysed using PyMOL and Discovery Studio visualizer v.3.1.

2.6. Anti-leishmanial activity assay

The effect of compound L1 on the viability of *L. donovani* AG83 promastigote cells was determined by standard 3-(4,5-dimethylthiazol-2-yl)-2,5-diphenylterazolium bromide (MTT) assay. The assay was performed as described previously with minor modifications [54, 55]. To mimic the leishmanial auto-phagosomal pathway, the assay was performed on low pH adapted promastigotes. For adaptation to lower pH, *L.donovani* Ag83 promastigotes were seeded gradually to M199 medium with Hanks salt at pH 7.0, 6.5, 6.0 and 5.5 with 15% FBS and incubated at 25 ^{o}C in a BOD incubator. After second passage at pH 5.5, cells were used for MTT assay. At the exponential phase (~1x10^{7} cells/ml), cells were collected by centrifugation at 1000xg and were resuspended in fresh M199 medium with 15% FBS to make 2.22 x10^{6} cells/ml. 90 µl of cells (2x10^{5} cells) were seeded in each well of three 96 well plates and incubated at

25°C in BOD incubator. After 1 hour, cells were treated with equal volume of L1 (10µl) at different concentrations and a known concentration (135 nM) of Amphotericin B as control. Plates were incubated at 25°C in BOD incubator. After 48 and 72 hours, plates were treated with MTT solution (5 mg/ml in PBS) with 10 µl added in each well. After incubating at 25°C for 3 hours, 100 µl of stop solution (50% isopropanol and 10% SDS) were added to each well and left for incubation for another 15 minutes. Following incubation, the optical density at 570 nm was recorded in a microplate reader and the percentage cytotoxicity was calculated with respect to untreated control cells.

3. Results and discussion

3.1 Sequence alignment and model building

Comparative genome analysis highlighted the presence of putative L-asparaginase gene only in few enteric protozoa (**Supplementary Table 1**). In case of *Leishmania donovani*, interestingly two gene fragments coding for L-asparaginase were found. One of these present at chromosome number 15, has been annotated as the cytoplasmic L-asparaginase in the UniProt (E9BC85) database, possibly corresponding to bacterial Type I enzyme. The other (putative) may therefore correspond to the Type II bacterial L-asparaginase (**Supplementary figure 1a**). Thus, the presence of L-asparaginase gene may signify its important role in the metabolism and survival of organisms possessing it. On comparing the protein sequences of L-asparaginases from various Leishmania genomes with that of bacterial L-asparaginases, a high degree of conservation was noted (**Figure 1**). However, few crucial differences were also identified including Tyr to Ala replacement in catalytic triad I. The other variations and their interpretations are discussed in detail in the following sections.

The human L-asparaginase (HLA) belongs to Type III family, representing a substantially different class and catalytic mechanism as compared to bacterial and protozoan L-asparaginases [45]. Moreover, there is negligible sequence similarity between HLA and LdAI (BLASTp, E

value 1.8). Assuming that LdAI is an essential enzyme for Leishmania, inhibiting its function will selectively prevent the survival of the pathogen without adversely affecting the human host. This projects LdAI a promising candidate for rational design of selective inhibitors. To study similarity/dissimilarity among various L-asparaginases, structural model of LdAI was generated, using EcAI as template (sequence identity 37%). The Ramachandran plot of the modeled LdAI structure showed 92.5% residues in the most favourable region, 6.2% in the allowed region, and 0.4% in the disallowed region (**Supplementary figure 1b**). This was very similar to the EcAI template (Pdb id: 2p2d) that showed the presence of 92.2% residues in most favourable region, 7.4% in the allowed region, none in the disallowed region. For LdAI, it was suspected that the residues present in the disallowed region (0.4%) could represent the active site amino acids. A PROCHECK analysis however, suggested that they are not. Further, PROCHECK analysis showed that the main-chain and side-chain parameters were also satisfactory, thus confirming the reliability of the LdAI structure. Finally, the ProSA analysis of energy criteria showed negative interaction energies for most of the residues in LdAI, confirming a stable structure (**Supplementary figure 1c**).

3.2 MD simulations of apo- and holo-enzyme

In the absence of a crystal structure of LdAI, MD simulations of its apo- and holo- form provided preliminary insights on its 3D conformation. The simulations of the apo- and holo-forms were carried out for 10 ns each till the backbone RMSD stabilized (**Supplementary figure 2a**). Furthermore, comparative stability of the enzyme in the absence and presence of its substrate was confirmed by consistency in total energy (potential, kinetic and columbic energies) of both the apo- and holo- forms during the entire simulation time (**Supplementary figure 2b**). On analyzing the overall structural scaffold, it was evident that the LdAI monomer was very similar to those of the related asparaginases. Each LdAI monomer is composed of two distinct α/β domains connected by an un-structured linker (**Figure 2**). The larger N-terminal domain (Green) comprises

of 10 β-pleated sheet and 3 α-helices along with a rigid hairpin composition at the active site loop (residues 11-27 in modelled structure). This is followed by a 21 residue (residues 187-207 in modelled structure) linker region (Grey) containing a β-sheet that extends to the C-terminal domain consisting 2 β-pleated sheets and 4 α-helices (Magenta). As a whole, the secondary structure content is similar to the other reported type I enzymes *i.e.* E. *coli* and *Pyrococcus horikosshi* (PhA) [46, 47]. The similarity in secondary structural folds is evident from the high degree of superimposition of EcAI and LdAI models (**Supplementary Figure 3a**). Similar to bacterial and archeal L-asparaginases, LdAI also exhibited two oppositely oriented active sites along the vertical axis [48].

Moreover, the C-terminal domain has six extra amino acids protruded out of the globular structure when compared to EcAI (**Supplementary Figure 3b**). It can be hypothesized that the C-terminal tail is essential for inter-domain stabilization and consequently formation of higher order oligomeric assemblies. Furthermore, the linker region was found structured and comparatively longer in LdAI. Since, *Leishmania* is an early eukaryote; the linker domain might confer flexibility to C-terminal and N-terminal domains, thus modulating macromolecular associations and subsequently biological functions. This is in accord with hypothesis by Wang *et al.,* which sheds light on role of terminal tails and varied length of internal linkers on eukaryotic, bacterial and archaeal proteome [49]. These non domain regions play a crucial role in stabilization of macromolecular complexes and higher order tertiary structures through various non bonding interactions. Also, a rigid β-hairpin loop at the active site was suggestive of limited flexibility and restricted solvent accessibility to the catalytic site (**Figure 2**). This might confer LdAI with activity similar to the one seen in case of EcAI and PhA [48]. We confirmed this from solvent accessible surfaces of the loop region in LdAI. The comparably similar solvent accessibility hints toward similar activity (EcAI 208 $Å^2$, EcA II 264 $Å^2$, LdAI 240 $Å^2$). Moreover, the comparative analysis of solvent accessibility of the entire active site pocket also showed similar results (**Supplementary Figure 3c**).

3.3 Active site

Previously reported L-asparaginase crystal structures have shown the presence of two catalytic triads (I and II) at each active site. The triad I is composed of a nucleophile (Thr), a base (Tyr) and a acidic moiety (Glu) which functions on the flexibility of active site loop. Similarly, triad II is also composed of a second nucleophile (Thr) that activates a water molecule along with a basic (Lys) and an acidic residue (Asp). These two triads function in a concerted manner and convert the substrate asparagine into aspartate in the presence of a water molecule (acting as second nucleophile) [50].

The multiple sequence alignment of all available Leishmania L-asparaginase sequences along with the bacterial L-asparaginase (EcAI and EcAII) yielded interesting insights on active site conformation of LdAI (**Figure 1**). There were significant overlaps in the conserved residues of Leishmania asparaginases and the bacterial asparaginases (Red). The first nucleophile in triad I (Thr 38) along with the entire triad II (Asp 116, Thr 117 and Lys 187) were found conserved (Red). However, few evolutionary replacements in the LdAI active site make its active site conformationally different from the known asparaginases. The crucial tyrosine moiety (residue 24 on active site loop) of EcAI is found replaced with an alanine (residue 48 on active site loop) of LdAI (Green star, figure 1). Previous studies on bacterial asparaginases have shown that flipping of this tyrosine residue inside and outside the plain is responsible for activating the nucleophilic threonine residue that attacks the substrate [51, 52]. Hence, an alanine replacement in LdAI (Tyr 48--->Ala) creates a certain degree of muddiness on the mechanism of action of this enzyme.

For deciphering this, we did a rigorous sequence and structure analysis of the simulated structure. We found that there were two lysine residues on the active site loop that were conserved in the Leishmania asparaginases (highlighted in magenta, **Figure 1**). However, on closer look at their structural orientations, only the Lys 43 was found in plane of the triad I. Further, we delved into identifying a possible acidic residue that must interact with the base

lysine so as to activate it. From the sequence alignment, it was found that glutamic acid (301' chain B, highlighted in orange, **Figure 1**) was conserved in all type I Leishmania asparaginases. Interestingly, this residue is also found conserved for most other type II asparaginases [50] (Green star). This led us to hypothesise that Leishmania being an early eukarya shares the structural and sequence motifs of both type I and type II asparaginases. Hence, we propose the presence of a different version of active site residues working in consort to bring upon substrate conversion in LdAI (**Figure 3a**). The major difference being at the triad I where the base Lys 43 after getting deprotonated by acid Glu 301' activates the first nucleophile Thr 38 that attacks the substrate L-asparagine.

We confirmed our results by performing simulations of LdAI in presence of its substrate asparagine (-holo enzyme). Interestingly, it was found that the β-hairpin loop at the active site underwent reorganization and became flexible in presence of asparagine (**Figure 3b**). The flexibility of the active site loop gave support to our hypothesis that glutamic acid (residue 301') de-protonates the base lysine (residue 43) which in turn activates the nucleophile (Thr 38). The comparison of RMSF of the apo- and holo- enzymes further confirmed the stabilization of entire protein on substrate binding (**Supplementary figure 2a, 2b**) and reorganization of active site loop leading to increase of flexibility at the loop region (**Figure 3c**). This finding is in contrast to the previous reports that suggested mobile gate mechanism of active site loop where opening and closing of the loop was found ligand-dependent [53]. Interestingly, we have recently reported similar reorganization of structured active site loop in another type I asparaginases (P. *furiosus*) that assists substrate entry and its conversion to product [56]. Therefore, LdAI appears to employ a distinct mechanism of action and warrants further investigation. Interestingly, a recently reported L-asparaginase from *Mycobacterium tuberculosis* (*MyAnsA*) shows a similar Val substitution for Tyr [26]. Such a finding is pertinent in the context of *Leishmania* survival inside the phagolysosome. *Leishmania* probably involves an analogous mechanism of action to neutralize the acidic environment as is done by MyAnsA of *Mycobacterium*.

3.4 Virtual screening of compounds against LdAI

The initial library of compounds was created by screening substances from ZINC database that had 90% similarities in structural and physicochemical parameters with L-asparagine. The resulting 11,438 drug-like ligands were identified and retained for the receptor based screening. The compounds showing higher binding scores compared to L-asparagine were then filtered based on the Lipinski's rule of five and relative iDock scores. Only the top 100 screened compounds possessing higher binding affinities as compared to the original substrate L-asparagine (>-5.3 kcal/mole, score for L-asparagine) were selected. Following this, second screening was done to identify 20 potential candidate molecules on the basis of their lower toxicity profiles (LD50<2.5 mol/kg). Final screening step involved free energy calculations and comparative binding studies with HLA using MOE. This resulted in five compounds showing higher binding energies with LdAI as compared to HLA (**Table 1**, **Supplementary figure 4**). The compounds are as follows: compound L1 (ZINC 565127), compound L2 (ZINC 9013886), compound L5 (ZINC 86862222), compound L7 (ZINC 83260818) and compound L12 (ZINC 58950950) (**Figure 4**). All these potential inhibitors were successfully filtered by Lipinski's rule of five (**Table 1**) and various ADMET parameters (**Table 2**) using admetSAR (**Supplementary methods**). These ligands screened on the basis of similarity with substrate showed favorable interactions at the enzyme's active site (**Figure 5**, **Supplementary figure 5)**. This is because of the extra number of non-covalent bonding interactions at the active site pocket, resulting in more stable enzyme-inhibitor complexes.

All five compounds showed excellent probabilities for intestinal absorption and minimal permeability for blood brain barrier (>0.7). The caco-2 permeability scores indicating moderate paracellular movement of compounds across the intestinal monolayers also aid in drug-likeliness of the five compounds. Moreover, owing to their moderate P-glycoprotein substrate propensities (~0.6) and high CYP2D6 inducing probabilities (>0.9) , all five compounds are predicted to have

moderate chances of drug efflux with higher probability of forming active metabolite. Thus, the ADMET profiles of the screened compounds suffice appropriate pharmacokinetic parameters and have reasonable druggability for using as potential drug candidates. In the absence of any previous reports on inhibition of leishmanial L-asparaginase, these identified compounds await in-vitro and in-vivo testing for their effectiveness against leishmaniasis.

3.5 Ligand L1

The ligand L1 corresponding to ZINC ID 565127 is recognized by IUPAC name 2-{3-[2-(3-aminophenyl)-2-oxoethyl]-3-hydroxy-2-oxo-2,3-dihydro-1H-indol-1-yl}acetamide. With net zero charge under physiological conditions, it binds to the primary nucleophile Thr 38 of catalytic triad I through a hydrogen bond between its HG1 and O1. The bulky indole ring gets accommodated inside the active site groove and is further stabilized by five hydrogen bonds with four active site residues at the periphery i.e. Leu 49, Ser86, Met41 and Asp85 (**Figure 5a**).

3.6 Ligand L2

The ligand L2 corresponding to ZINC ID 9013886 is recognized by IUPAC name 2-amino-4-hydroxy-5-(4-hydroxy-3-methoxyphenyl)-5, 8-dihydropyrido [2, 3-d] pyrimidin-7 (6 H)-one. With net zero charge under physiological conditions, it binds to the primary nucleophile Thr 38 of catalytic triad I through hydrogen bonding between its HG1 and O1. Additional hydrogen bonding with six other residues of the active pocket that include Leu 49, His 192, Asp 85 and Ser 87 along with Asp 118 and Met 144, belonging to triad II groove (**Figure 5b**).

3.7 Ligand L5

The ligand L5 corresponding to ZINC ID 86862222 is recognized by IUPAC name 3, 3'-diamino-4, 4'-dihydroxydiphenyl sulfone. With net zero charge under physiological conditions, it binds to the primary nucleophile Thr 38 of catalytic triad I through dual-hydrogen bonding between OG1 and H13 and H14 moieties of L5. The bulky phenyl ring helps in stabilization of L5 inside the active site groove. The protein-ligand complex is further stabilized by nine additional hydrogen bonds between L5 and Asp 85, Ser 86 and Asp 118 residues belonging to

the active site pocket of the protein (**Figure 5c**).

3.8 Ligand L7

The ligand L7 corresponding to ZINC ID 83260818 is recognized by IUPAC name N-[(2R,3S,4R,5S,6R)-2,4,5-trihydroxy-6-(hydroxymethyl)-4-(1H-indol-3-yl)tetrahydropyran-3yl] acetamide. With net zero charge under physiological conditions, L7 also binds to the primary nucleophile Thr 38 of catalytic triad I through dual-hydrogen bonding between HG1 and O2 and O5 of L7. Additionally, another hydrogen bond between OG1 of Thr 38 and H2 of the ligand L7 exists. Besides these essential hydrogen bonds, the protein-ligand complex is further stabilized by five additional hydrogen bonds with Leu 49, Glu 50, Asp 85 and Asp 118 residues of LdAI active site (**Figure 5d**).

3.9 Ligand L12

The ligand L12 corresponding to ZINC ID 58950950 is recognized by IUPAC name 6-amino-3-methyl-4-(5-methyl-2-furyl)-1, 4-dihydropyrano [2, 3-c] pyrazole-5-carboxamide. With net zero charge under physiological conditions, it strongly binds to the primary nucleophile Thr 38 of catalytic triad I via hydrogen bonding between its OG1 and H8, H9 and H10. The stability of this complex is further stabilized by seven additional hydrogen bonds with five residues at active site pocket that include Leu49, Glu50, Asp85 along with Asp118 and Met114 belonging to triad 2 pocket (**Figure 5e**).

3.10 MD simulations and the overall stability of structure

To validate the stability of enzyme-inhibitor complexes obtained from docking studies, MD simulations were carried up to 10 ns as described previously in the methods section. In the presence of ligands, the backbone RMSD stabilized after 6 ns, indicating stabilization of docked complex in all cases (**Figure 6**). Changes in radius of gyration over the simulation indicate folding behavior of the protein. In case of both docked and native LdAI, radius of gyration varied between 2.6 nm and 2.7 nm (**Figure 7**). This suggests that the binding of the ligands to

LdAI enzyme does not affect the original protein architecture. However, in physiological conditions, enzymes are dynamic in nature. While some regions are static in nature, others confer flexibility to the enzymes to carry specific functions. RMSF analysis of Cα atoms of the protein during last 4 ns of simulation of docked complexes revealed residues contributing to regions of higher flexibility in the enzyme (**Figure 8**). The analysis of active site loop region in the complexes showed that in case of L1, L7 and L12 ligands, comparatively lower residue-fluctuation was present (dotted rectangle, Figure 3). Finally, total energy profile of the enzyme-ligand complexes during the entire simulation was also analyzed to ascertain the overall stability of the systems in terms of potential, kinetic and columbic energies. It was observed that all five complexes showed constant energy profile during the trajectory of simulation (**Supplementary Figure 6**). So, based on strong hydrogen bonding interactions at the active site groove that remained throughout the MD simulation trajectory, these five identified compounds show excellent stability and reliability.

3.11 Assessment of anti-leishmanial activity

Following the stringent screening criteria, we examined the anti-leishmanial activity of one of the five identified compounds. On testing, L1 showed appreciable reduction in cell viability of *L. donovani* AG83 promastigote cells in a dose dependent manner. At 72 hours, the inhibitory effect was comparable to that of the standard drug (Amphotericin B) **(Figure 9)**. Although the dose requirement was on the higher side but given the ADMET criteria of selecting relatively low toxicity compounds, L1 appears promising. Overall, these results represent a starting point of rigorous in *vivo* experimentation for developing newer and potent drugs from the identified anti-leishmanial target.

Conclusions

In the present study, we have explored the possibility of targeting L-asparaginases in pathogenic

Leishmania donovani (LdAI) as a new therapeutic strategy against lesihmaniasis. Based on our sequence and structural analysis, we report a novel mechanism of active site remodelling involving different residues at the active site as compared to previously reported asparaginase. Following this, we screened a large library of compounds for identifying inhibitors which could favourably interact with the active site of LdAI. Based on an integrated approach involving molecular modelling, docking and MD simulations, we selected five compounds which could strongly bind at the LdAI active site. The binding mode analysis of all five compounds showed the presence of a strong hydrogen bonding network involving the active site residues. To the best of our knowledge this is a firsthand report on targeting L-asparaginase in a pathogenic protozoan.

The major conclusions of this study are as follows: (1) A comparison with previously reported asparaginases revealed flexible domain architecture of LdAI, owing to longer inter-domain linker length. (2) The catalytic triad I of LdAI constitutes different residues (Lys 43 as base, Glu 301' as acid and Thr 38 as nucleophile), not reported in other L-asparaginases. (3) The rigid active site loop of LdAI gets un-structured in the presence of substrate, possibly enhancing substrate accessibility. (4) The selected inhibitors showed high affinity to LdAI and are devoid of any significant affinity to the human asaparaginase. (5) The heterocyclic rings in the five identified inhibitors help in stabilization at the active site groove along with the hydrogen bonding with the surrounding residues. (6) Compound L1 works at a higher dose but produces comparable anti-leishmanial activity as that of standard compounds. In summary, these mechanistic insights on functioning of pathogenic protozoan L-asparaginase can help deciphering the survival strategies of these organisms and hence can also aid in developing novel therapeutic strategies. The preliminary results suggest that the identified lead molecules, may serve as models for developing new and efficient inhibitors against leishmaniasis.

Acknowledgement

This work was supported financially and infrastructurally by IIT Delhi. JS and AS acknowledge

the financial support received from IIT Delhi and ICMR India, respectively. PJ, Md. IK and KKS acknowledge the financial and infrastructural support of NIPER Hajipur. The authors also acknowledge Banpreet Kaur and Vimal Kant for technical discussions and suggestions.

References

[1] Kaye, P., Scott, P. Leishmaniasis: complexity at the host-pathogen interface. Nat Rev Microbiol. 2011, 9, 604-15.

[2] Guerin, P.J., Olliaro, P., Sundar, S., Boelaert, M., Croft, S.L., Desjeux, P., et al. Visceral Leishmaniasis: current status of control, diagnosis, and treatment, and a proposed research and development agenda. Lancet Infect Dis. 2002, 2, 494-501.

[3] Croft, S.L., Coombs, G.H. Leishmaniasis-current chemotherapy and recent advances in the search for novel drugs. Trends Parasitol. 2003, 19, 502-8.

[4] Fernandez-Guerrero, M.L., Aguado, J.M., Buzon, L., Barros, C., Montalban, C., Martin, T., et al. Visceral leishmaniasis in immunocompromised hosts. Am J Med. 1987, 83, 1098-102.

[5] Reiner, S.L., Zheng, S., Wang, Z.E., Stowring, L., Locksley, R.M. Leishmania promastigotes evade interleukin 12 (IL-12) induction by macrophages and stimulate a broad range of cytokines from CD4+ T cells during initiation of infection. The Journal of experimental medicine. 1994, 179, 447-56.

[6] Tiuman, T.S., Santos, A.O., Ueda-Nakamura, T., Filho, B.P., Nakamura, C.V. Recent advances in leishmaniasis treatment. Int J Infect Dis. 2011, 15, e525-32.

[7] Cunningham, A.C. Parasitic adaptive mechanisms in infection by leishmania. Experimental and molecular pathology. 2002, 72, 132-41.

[8] Vannier-Santos, M.A., Martiny, A., de Souza, W. Cell biology of Leishmania spp.: invading and evading. Current pharmaceutical design. 2002, 8, 297-318.

[9] Frezard, F., Demicheli, C., Ribeiro, R.R. Pentavalent antimonials: new perspectives for old drugs. Molecules. 2009, 14, 2317-36.

[10] New, R.R., Chance, M.L., Heath, S. Antileishmanial activity of amphotericin and other antifungal agents entrapped in liposomes. The Journal of antimicrobial chemotherapy. 1981, 8, 371-81.

[11] Olliaro, P.L., Bryceson, A.D. Practical progress and new drugs for changing patterns of leishmaniasis. Parasitol Today. 1993, 9, 323-8.

[12] Bell, C.A., Cory, M., Fairley, T.A., Hall, J.E., Tidwell, R.R. Structure-activity relationships of pentamidine analogs against Giardia lamblia and correlation of antigiardial activity with DNA-binding affinity. Antimicrobial agents and chemotherapy. 1991, 35, 1099-107.

[13] Bell, C.A., Hall, J.E., Kyle, D.E., Grogl, M., Ohemeng, K.A., Allen, M.A., et al. Structure-activity relationships of analogs of pentamidine against Plasmodium falciparum and Leishmania mexicana amazonensis. Antimicrobial agents and chemotherapy. 1990, 34,1381-6.

[14] Smith, A.C., Yardley, V., Rhodes, J., Croft, S.L. Activity of the novel immunomodulatory compound tucaresol against experimental visceral leishmaniasis. Antimicrobial agents and chemotherapy. 2000, 44, 1494-8.

[15] Afonso, L.C., Scharton, T.M., Vieira, L.Q., Wysocka, M., Trinchieri, G., Scott, P. The adjuvant effect of interleukin-12 in a vaccine against Leishmania major. Science. 1994, 263, 235-7.

[16] St George, S., Bishop, J.V., Titus, R.G., Selitrennikoff, C.P. Novel compounds active against Leishmania major. Antimicrobial agents and chemotherapy. 2006, 50, 474-9.

[17] van Griensven, J., Diro, E., Lopez-Velez, R., Boelaert, M.et al. HIV-1 protease inhibitors for treatment of visceral leishmaniasis in HIV-co-infected individuals. Lancet Infect Dis. 2013,13, 251-9

[18] Jha, T.K., Sundar, S., Thakur, C.P., Bachmann, P., Karbwang, J., Fischer, C., et al. Miltefosine, an oral agent, for the treatment of Indian visceral leishmaniasis. N Engl J Med. 1999, 341, 1795-800.

[19] Soto-Mancipe, J., Grogl, M., Berman, J.D. Evaluation of pentamidine for the treatment

of cutaneous leishmaniasis in Colombia. Clin Infect Dis. 1993, 16, 417-25.

[20] Sundar, S., Jha, T.K., Sindermann, H., Junge, K., Bachmann, P., Berman, J. Oral miltefosine treatment in children with mild to moderate Indian visceral leishmaniasis. The Pediatric infectious disease journal. 2003, 22, 434-8.

[21] Florens, L., Washburn, M.P., Raine, J.D., Anthony, R.M. et.al. A proteomic view of the Plasmodium falciparum life cycle. Nature. 2002, 419, 520-6.

[22] Damte, D., Suh, J.W., Lee, S.J., Yohannes, S.B., Hossain, M. A., Park, S.C. Putative drug and vaccine target protein identification using comparative genomic analysis of KEGG annotated metabolic pathways of Mycoplasma hyopneumoniae. Genomics.2013, 102, 47-56.

[23] Manhas, R., Tripathi, P., Khan, S., Sethu Lakshmi, B., Lal, S.K., Gowri, V.S., Sharma, A., Madhubala, R. Identification and functional characterization of a novel bacterial type asparagine synthetase A: a tRNA synthetase paralog from Leishmania donovani. J Biol Chem. 2014, 289, 12096-108.

[24] Bansal, S., Gnaneswari, D., Mishra, P., Kundu, B. Structural stability and functional analysis of L- Asparaginase from Pyrococcus furiosus, Biochemistry (Moscow). 2010, 75, 375-381.

[25] St George, S., Bishop, J.V., Titus, R.G., Selitrennikoff, C.P. Novel compounds active against Leishmania major. Antimicrobial agents and chemotherapy. 2006, 50, 474-9.

[26] Gouzy, A., Larrouy-Maumus, G., Bottai, D., Levillain, F., Dumas, A., Wallach, J.B., et al. Mycobacterium tuberculosis exploits asparagine to assimilate nitrogen and resist acid stress during infection. PLoS Pathog. 2014, 10, e1003928.

[27] Larkin, M.A., Blackshields, G., Brown, N.P., Chenna, R., McGettigan, P.A., McWilliam, H., et al. Clustal W and Clustal X version 2.0. Bioinformatics. 2007, 23, 2947-8.

[28] McWilliam, H., Li, W., Uludag, M., Squizzato, S., Park, Y.M., Buso, N., et al. Analysis Tool Web Services from the EMBL-EBI. Nucleic acids research. 2013, 41, W597-600.

[29] Goujon, M., McWilliam, H., Li, W., Valentin, F., Squizzato, S., Paern, J., et al. A new

bioinformatics analysis tools framework at EMBL-EBI. Nucleic acids research. 2010, 38, W695-9.

[30] Y, Zhang. I-TASSER server for protein 3D structure prediction. BMC Bioinformatics. 2008, 9, 40-48.

[31] Roy, A., Kucukural, A., Zhang, Y. I-TASSER: a unified platform for automated protein structure and function prediction. Nature Protocols. 2010, 5, 725-738.

[32] Laskowski, R.A., Rullmannn, J.A., MacArthur, M.W., Kaptein, R., Thornton, J.M. AQUA and PROCHECK-NMR: programs for checking the quality of protein structures solved by NMR. Journal of biomolecular NMR. 1996, 8, 477-86.

[33] Wiederstein, M., Sippl, M.J. ProSA-web: interactive web service for the recognition of errors in three-dimensional structures of proteins. Nucleic acids research. 2007, 35, W407-10.

[34] Trott, O., Olson, A.J. AutoDock Vina: improving the speed and accuracy of docking with a new scoring function, efficient optimization, and multithreading. Journal of computational chemistry. 2010, 31, 455-61.

[35] Hongjian, L., Leung, K., Ballester, PJ., Wong, M. istar: A Web Platform for Large-Scale Protein-Ligand Docking. *PLoS ONE*, 2014, 9, e85678.

[36] Lipinski, C.A. Chris Lipinski discusses life and chemistry after the Rule of Five. Drug discovery today. 2003, 8, 12-6.

[37] Cheng, F., Li, W., Zhou, Y., Shen, J., Wu, Z., Liu, G., et al. admetSAR: a comprehensive source and free tool for assessment of chemical ADMET properties. Journal of chemical information and modeling. 2012, 52, 3099-105.

[38] Vilar, S., Cozza, G., Moro, S. Medicinal chemistry and the molecular operating environment (MOE): application of QSAR and molecular docking to drug discovery. Current topics in medicinal chemistry. 2008, 8, 1555-72.

[39] Morris, G. M., Huey, R., Lindstrom, W., Sanner, M. F., Belew, R. K., Goodsell, D. S. and Olson, A. J. Autodock4 and AutoDockTools4: automated docking with selective receptor

flexiblity. J. Computational Chemistry 2009, 16, 2785-91.

[40] Halgren, T. A., Murphy, R. B., Friesner, R. A., Beard, H. S., Frye, L. L., Pollard, W. T., Banks, J. L. Glide: A New Approach for Rapid, Accurate Docking and Scoring. 2. Enrichment Factors in Database Screening. J. Med. Chem. 2004, 47, 1750-59.

[41] Verdonk, M. L., Cole, J. C., Hartshorn, M. J., Murray, C. W., Taylor, R. D. Improved Protein-Ligand Docking Using GOLD. Proteins.2003, 52, 609-623.

[42] Feher, M., Williams CI. Effect of input differences on the results of docking calculations. J Chem Inf Model. 2009, 49, 1704-14.

[43] Pronk, S., Pall, S., Schulz, R., Larsson, P., Bjelkmar, P., Apostolov, R., et al. GROMACS 4.5: a high-throughput and highly parallel open source molecular simulation toolkit. Bioinformatics. 2013, 29, 845-54.

[44] Schüttelkopf, A. W., van Aalten, D. M. F. "PRODRG: a tool for high-throughput crystallography of protein-ligand complexes", Acta Crystallogr. 2004, D60, 1355–1363.

[45] Nomme, J., Su, Y., Konrad, M., Lavie, A. Structures of apo and product-bound human L-asparaginase: insights into the mechanism of autoproteolysis and substrate hydrolysis. Biochemistry. 2012, 51, 6816-26.

[46] Yao, M., Yasutake, Y., Morita, H., Tanaka, I. Structure of the type I L-asparaginase from the hyperthermophilic archaeon Pyrococcus horikoshii at 2.16 angstroms resolution. Acta crystallographica. Section D, Biological crystallography. 2005, 61, 294-301.

[47] Swain, A.L., Jaskolski, M., Housset, D., Rao, J.K., Wlodawer, A. Crystal structure of Escherichia coli L-asparaginase, an enzyme used in cancer therapy. Proc Natl Acad Sci U S A. 1993, 90, 1474-8.

[48] Bansal, S,. Srivastava, A., Mukherjee, G., Pandey, R., Verma, A.K, Mishra, P., Kundu, B. Hyperthermophilic asparaginase mutants with enhanced substrate affinity and antineoplastic activity: structural insights on their mechanism of action. FASEB J. 2012, 26, 1161-71.

[49] Wang, M., Kurland, C.G., Caetano-Anolles, G. Reductive evolution of proteomes and protein structures. Proc Natl Acad Sci U S A. 2011, 108, 11954-8.

[50] Mario Sanches, Sandra Krauchenco and Igor Polikarpov , Structure, Substrate Complexation and Reaction Mechanism of Bacterial Asparaginases. Current Chemical Biology.2007, 12, 75-86.

[51] Bagert, U., Rohm, KH., On the role of histidine and tyrosine residues in *E. coli* asparaginase. Chemical modification and 1H-nuclear magnetic resonance studies. Biochim Biophys Acta. 1989; 9991, 36-41.

[52] Derst, C., Wehner, A., Specht, V., Röhm, K.H. States and functions of tyrosine residues in Escherichia-coli asparaginase-II. Eur J Biochem. 1994, 224, 533-40.

[53] Aung, H.P., Bocola, M., Schleper, S., Röhm, K.H. Dynamics of a mobile loop at the active site of Escherichia coli asparaginase. Biochim Biophys Acta. 2000, 14812, 349-59.

[54] Mirzaie, M., Nosratabadi, S.J., Derakhshanfar, A., Sharifi, I. Antileishmanial activity of Peganum harmala extract on the in vitro growth of Leishmania major promastigotes in comparison to a trivalent antimony drug. Vet Arhiv. 2007, 77, 365-75.

[55] Niks, M., M, Otto. Towards an optimized MTT assay. J. Immunol. Methods. 1990, 130, 149-151.

[56] Tomar, R., Sharma, P., Srivastava, A., Bansal, S., Ashish., Kundu., B. Structural and functional insights into an archael L-asparaginase obtained through linker-less assembly of constituent domains. Acta Crystallogr D Biol Crystallogr. 2014, 70, 3187-97.

Figure and Table Legends

Figure 1. Multiple sequence alignment of L-asparaginase Type I sequences from available Leishmania genomes with bacterial Type I and Type II (EcAI and EcAII respectively). The fully conserved residues across the species are shown in red, residues conserved only in Leishmania are shown in pink, Glu 301' and Val 302' found conserved in all Leishmania sequences and EcAII only are highlighted in yellow. The green star represents crucial Tyr to Ala replacement in Leishmania L-asparaginases.

Figure 2. Homology modelled LdAI dimer after 15ns of MD simulation. The two monomers are shown in violet and green respectively. The dotted red box highlights dimer interface, with arrows indicating the two active sites formed at the dimer interface. Enlarged LdAI monomer (blue dotted line) showing domain architecture comprising of separate C-terminal domain (green), N-terminal domain (violet) and an unstructured linker (orange).

Figure 3. Proposed active site conformation of LdAI**. a)** Residue composition of triad I and triad II are shown by dotted red and blue lines, respectively. **b)** Secondary structure reorganization of the LdAI active site loop shown in dotted circle in its apo-(beta hairpin, cyan) and holo-(unstructured, green) forms. **c)** RMSF of last 4ns simulations of apo- and holo- LdAI is shown. The higher fluctuation in active site loop region of holo-enzyme (dotted rectangle) corresponds to highly flexible unstructured loop region.

Figure 4. Molecular structures of five identified small molecule inhibitors (L1, L2, L5, L7, and L12) against LdAI.

Figure 5. Molecular representation of active site-inhibitor complexes. Active site molecular interactions for each of the protein-inhibitor complexes is shown. **a)** L1; **b)** L2; **c)** L5; **d)** L7; and **e)** L12.

Figure 6. All atom RMSD of LdAI-inhibitor complexes. Different ligands are shown in different color codes.

Figure 7. Radius of gyration of backbone atoms of LdAI-inhibitor complexes. Different ligands are shown in different color codes.

Figure 8. RMSF of LdAI-inhibitor complexes. Different ligands are shown in different color codes. Black stars represent active site residues.

Figure 9. Cytotoxicity profile of compound L1 against *L. donovani* AG83 promastigote cells. Cell toxicity of different concentrations of L1 is represented as percentage of untreated control after 72 h treatment. Amphotericin B (135 nM) was used as positive control.

Table 1. Docking, binding free energy and Lipinski's parameters for the substrate and identified compounds.

Compound	Molecular weight (g/mol)	xlogP	iDock score	HBA	HBD	PSA(Å^2)	MOE ΔG_{bind} (kJ mol^{-1})
L-asparagine	132.11	-2.81	-5.37	5	5	110	-11.34
L1	339.35	-0.23	-6.13	7	5	126	-22.14
L2	302.29	-0.25	-6.17	8	5	130	-20.13
L5	266.32	-0.95	-5.92	5	6	110	-18.61
L7	336.34	-1.49	-6.27	8	6	135	-14.88
L12	274.28	-0.13	-5.98	7	5	120	-13.99

Table 2. ADMET parameters of identified inhibitors.

Compound	Blood-Brain Barrier(-)	Intestinal Absorption(+)	Caco-2 Permeability(-)	P-glycoprotein Substrate	CYP2D6 Inhibitor
L1	0.97	0.99	0.70	0.71	0.91
L2	0.98	0.99	0.50	0.68	0.91
L5	0.87	0.98	0.66	0.64	0.84
L7	0.98	0.89	0.63	0.66	0.93
L12	0.92	0.91	0.67	0.53	0.96

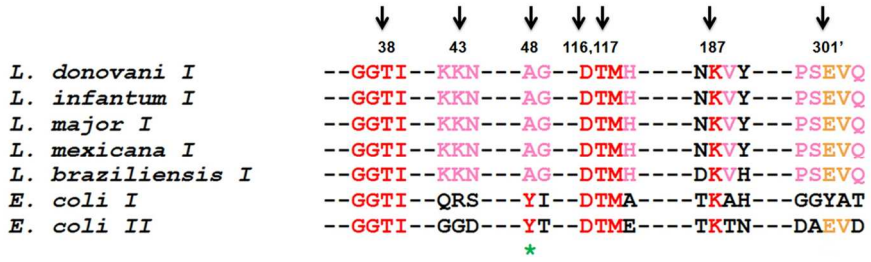

Multiple sequence alignment of L-asparaginase Type I sequences from available Leishmania genomes with bacterial Type I and Type II (EcAI and EcAII respectively). The fully conserved residues across the species are shown in red, residues conserved only in Leishmania are shown in pink, Glu 301' and Val 302' found conserved in all Leishmania sequences and EcAII only are highlighted in yellow. The green star represents crucial Tyr to Ala replacement in Leishmania L-asparaginases.
142x57mm (300 x 300 DPI)

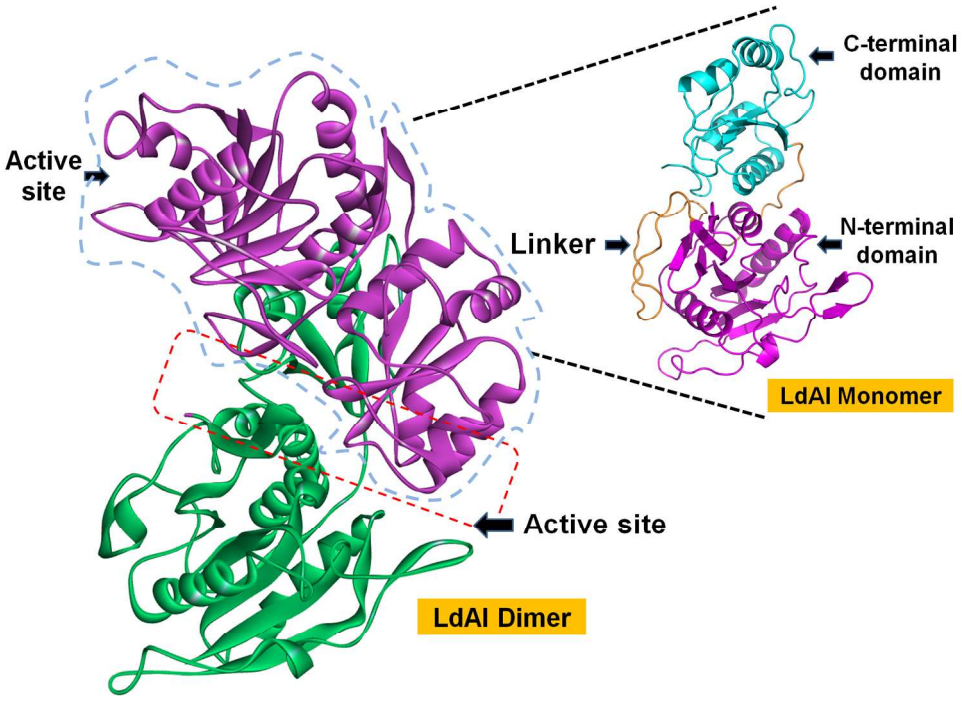

Homology modelled LdAI dimer after 15ns of MD simulation. The two monomers are shown in violet and green respectively. The dotted red box highlights dimer interface, with arrows indicating the two active sites formed at the dimer interface. Enlarged LdAI monomer (blue dotted line) showing domain architecture comprising of separate C-terminal domain (green), N-terminal domain (violet) and an unstructured linker (orange).
490x359mm (300 x 300 DPI)

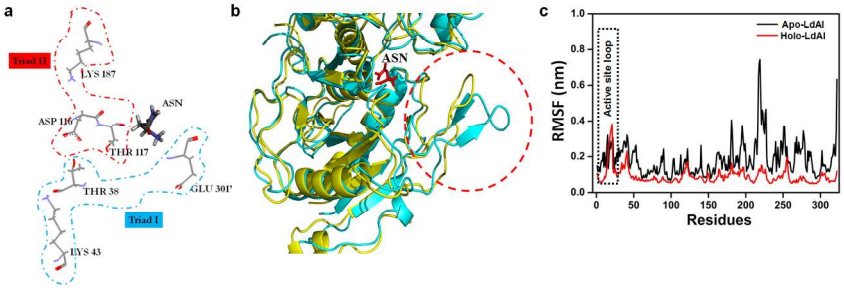

Proposed active site conformation of LdAI. a) Residue composition of triad I and triad II are shown by dotted red and blue lines, respectively. b) Secondary structure reorganization of the LdAI active site loop shown in dotted circle in its apo-(beta hairpin, cyan) and holo-(unstructured, green) forms. c) RMSF of last 4ns simulations of apo- and holo- LdAI is shown. The higher fluctuation in active site loop region of holo-enzyme (dotted rectangle) corresponds to highly flexible unstructured loop region.
542x187mm (300 x 300 DPI)

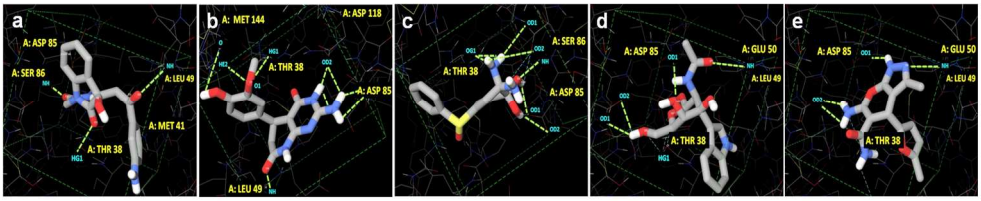

Molecular representation of active site-inhibitor complexes. Active site molecular interactions for each of the protein-inhibitor complexes is shown. a) L1; b) L2; c) L5; d) L7; and e) L12.
999x204mm (300 x 300 DPI)

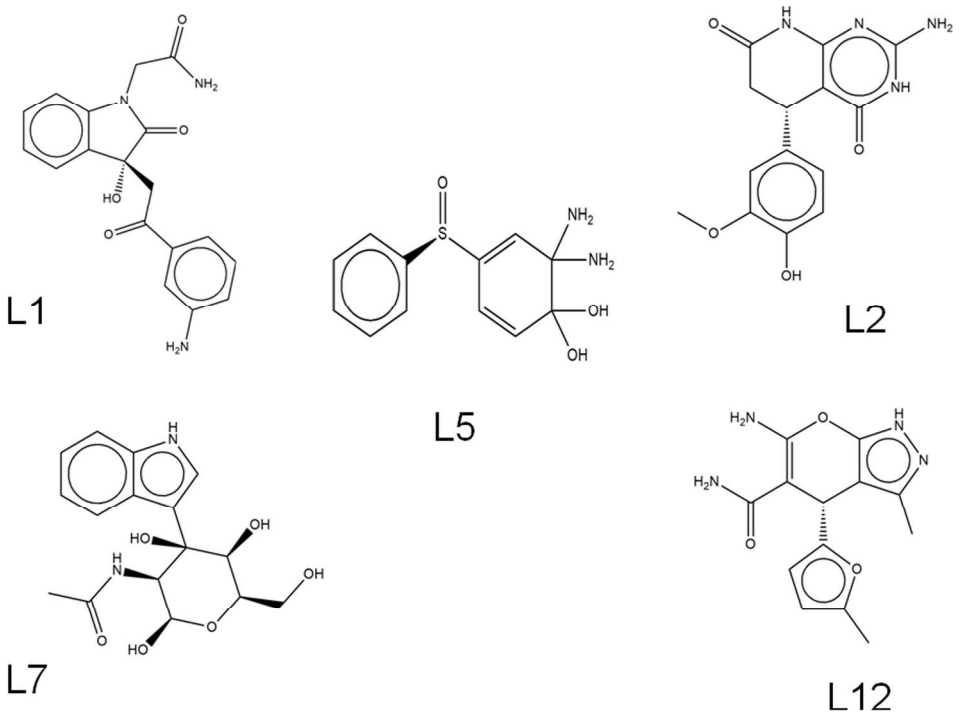

Molecular structures of five identified small molecule inhibitors (L1, L2, L5, L7, and L12) against LdAI.
252x203mm (300 x 300 DPI)

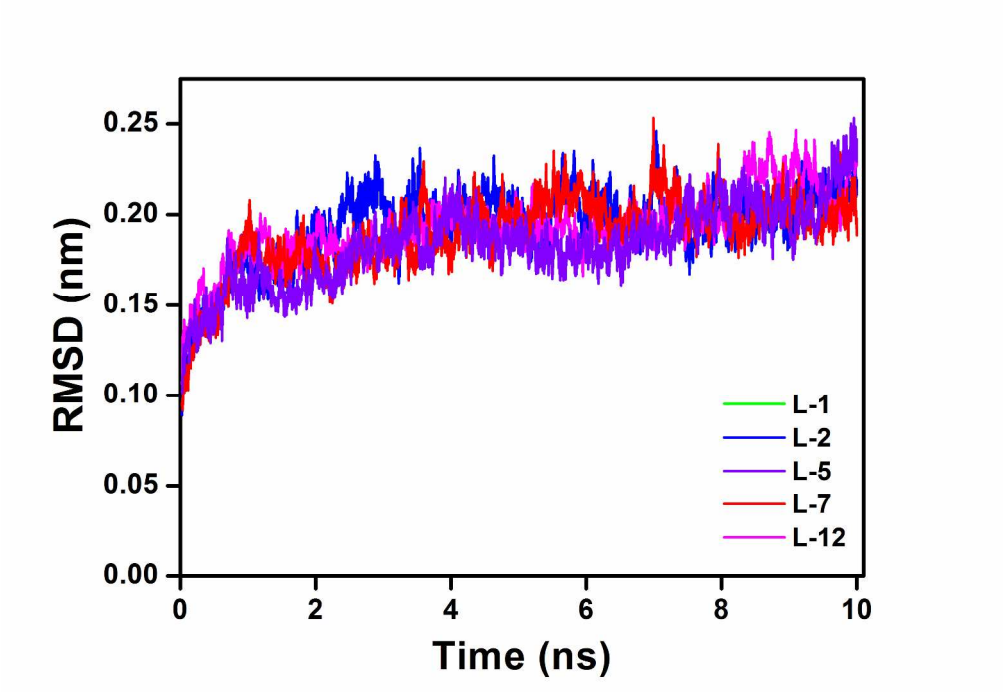

All atom RMSD of LdAI-inhibitor complexes. Different ligands are shown in different color codes.
288x200mm (300 x 300 DPI)

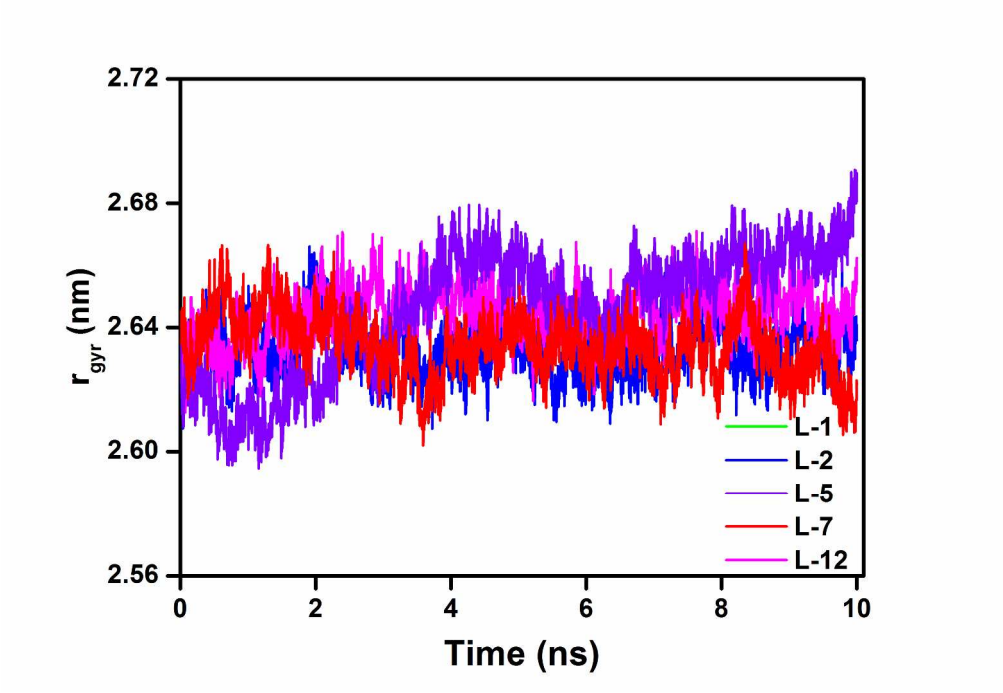

Radius of gyration of backbone atoms of LdAI-inhibitor complexes. Different ligands are shown in different color codes.
288x200mm (300 x 300 DPI)

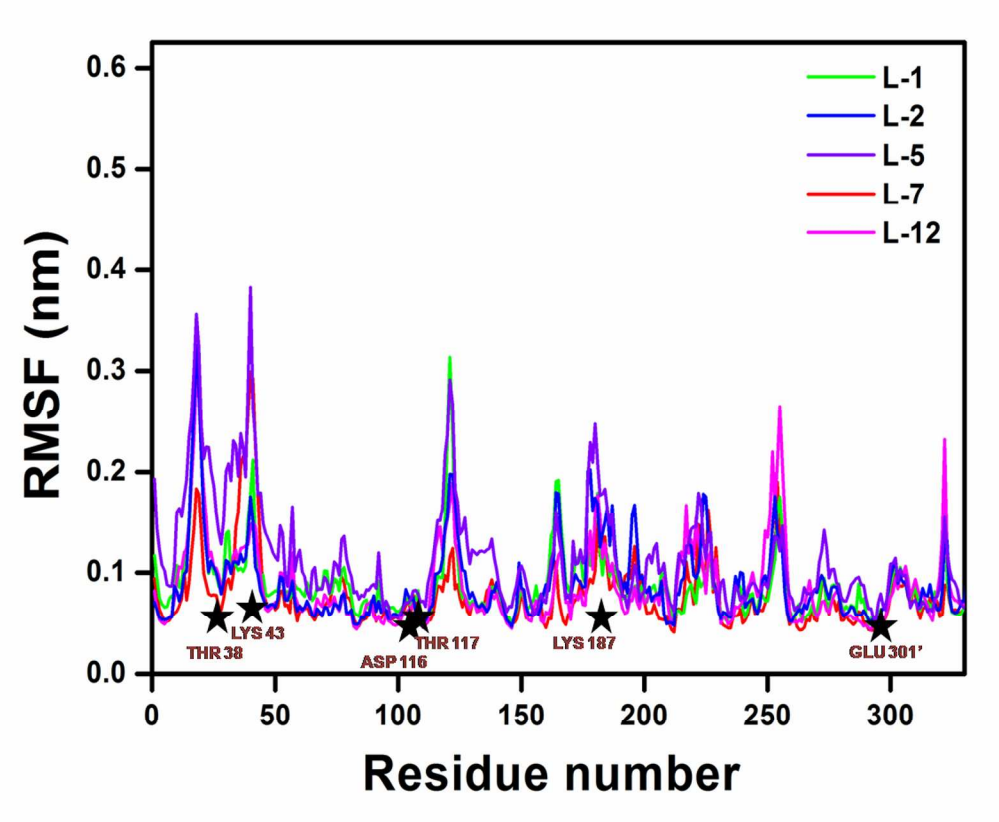

RMSF of LdAI-inhibitor complexes. Different ligands are shown in different color codes. Black stars represent active site residues.
298x246mm (300 x 300 DPI)

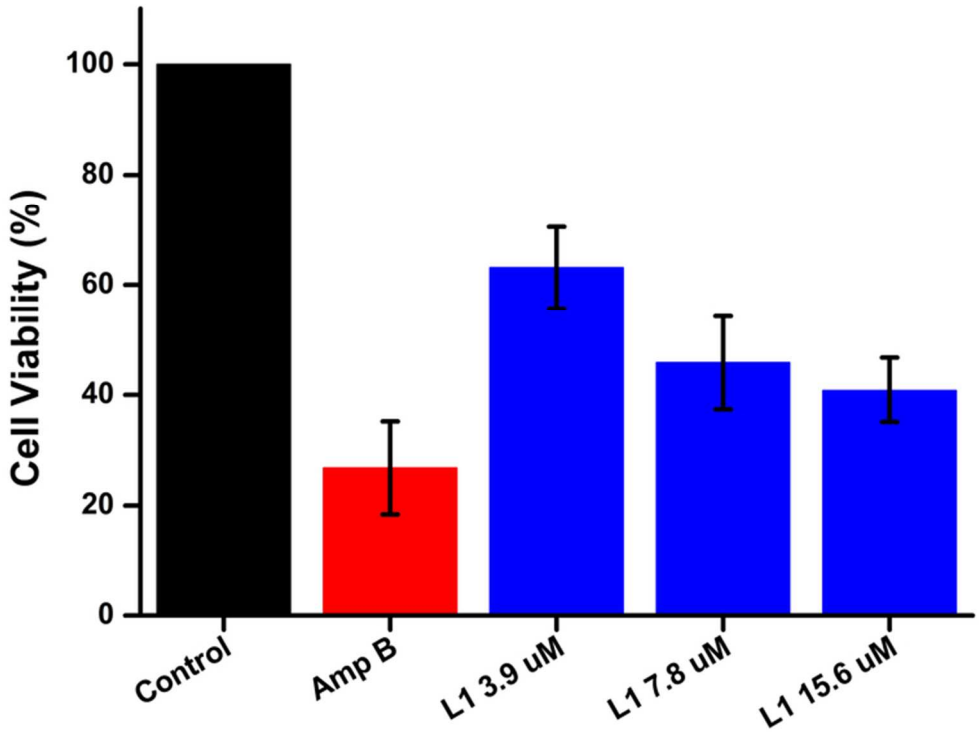

Cytotoxicity profile of compound L1 against L. donovani AG83 promastigote cells. Cell toxicity of different concentrations of L1 is represented as percentage of untreated control after 72 h treatment. Amphotericin B (135 nM) was used as positive control.
65x48mm (300 x 300 DPI)